CLAS-Analysis Note for the radiative decay of $\eta' \to \pi^+\pi^-\gamma$, with g11 data set

G. Mbianda Njencheu, I. Larin and M. Amaryan

Abstract

This note presents the analysis procedure, satistics and systematics of the radiative decay of $\eta' \to \pi^+\pi^-\gamma$ based on CLAS data collected during the photoproduction experiment $\gamma p \to p\eta'$ for the center-of-mass energy from 1.96 to 2.72 GeV at Jefferson Lab. The analysis is based on the highest statistics collected in this channel in comparison to other experiments reported so far. This analysis could provide an important test of the box anomaly, also accessible via the Primakoff reaction of $\pi^-\gamma^* \to \pi^-\pi^0$.

1 Introduction

The objective of this note is to report the radiative decay of the η' pseudoscalar meson which is governed by the chiral anomaly. Chiral anomaly is the non conservation of the axial vector current under quantization when gauge fields are present.

The anomalous decay of the π^0, also a pseudoscalar meson, was first measured in the 1960s [1] and have been updated in the recent years [2]. Moreover, many calculations were performed in this sector, see e.g. [3, 4]. Some of these decays are of special interest because their study permits a deep insight into aspects of modern physics.

By recent measurements of so-called η-factories, e.g. WASA@COSY [5] and KLOE [6], the decays of the η meson have become an important subject of modern hadron physics. Analogous to the π^0-decays, the theoretical calculations of the decays $\eta \to l^+l^-\gamma$, $\eta \to l^+l^-l^+l^-$ and $\eta \to l^+l^-$ can now be tested by modern measurements. While all the above mentioned decays proceed via the triangle anomaly, a study of the box anomaly is possible as well. This can be done by analyzing the decays $\eta' \to \pi^+\pi^-\gamma$ and $\eta' \to \pi^+\pi^-l^+l^-$. Ongoing measurements of the Primakoff process $\pi^-\gamma^* \to \pi^-\pi^0$ by COMPASS collaboration at CERN [7] could be used to verify the theoretical calculation of the transition form factor for the canonical anomalous process $\gamma^* \to \pi^+\pi^0\pi^-$ in a constituent quark loop model. The simplest contribution to this process is the quark "box" amplitude.

In the decay $\eta' \to \pi^+\pi^-l^+l^-$ CP-violation can be observed via asymmetry measurements of the $\pi^+\pi^-$- with respect to the l^+l^- decay planes.

In the η' sector experimental data are very scarce and only few theoretical calculations were done. However, the g11 and g12 experimental data from CLAS would introduce a significant contribution in this domain.

By theoretical extrapolation to the chiral point, all anomalous decays can be solely determined by the Wess-Zumino-Witten Lagrangian [8, 9].

2 Theoretical background

2.1 Pseudoscalar mesons

In the quark model the different hadrons are classified according to their quark content. Because these particles are color-neutral states, hadrons have to be constructed from a quark and an antiquark or three valence quarks (or antiquarks). The hadrons constructed by two valence quarks , a quark and an anti-quark with color and 'anti-color', respectively, are called mesons. The hadrons with three quarks with suitable colors are called baryons. These valence quarks give rise to the quantum numbers of the hadrons via their flavor and via their symmetry J^{PC}. Here $J = L + S$ is the total angular momentum containing orbital angular momentum L and spin S, while

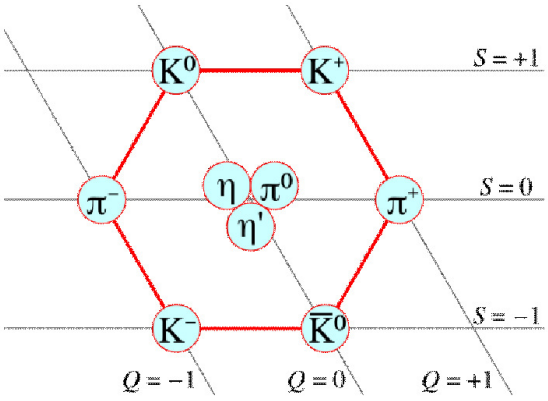

Figure 1: nonet of pseudoscalar mesons

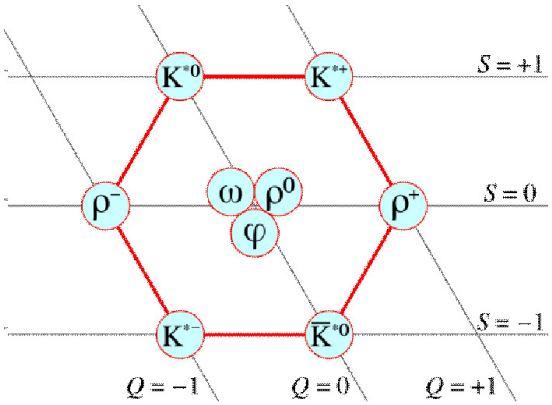

Figure 2: nonet of vector mesons

$P = (-1)^{L+1}$ and $C = (-1)^{L+S}$ stands for parity and charge conjugation. Baryons are constructed from three quarks, respectively, three antiquarks. Thus they are fermions. Mesons contain a quark-antiquark pair and thus are bosons. In the following work we are only interested in light mesons built by up, down or strange quarks, which are subject to an approximate U(3) flavor symmetry. The resulting nine states can be decomposed into a singlet and an octet state.

The different mesons can be classified into types according to their spin configurations.

Type	S	L	P	J	J^P
Pseudoscalar meson	0	0	-	0	0^-
Axial vector meson	0	1	+	1	1^+
Vector meson	1	0	-	1	1^-
Scalar meson	1	1	+	0	0^+
Tensor meson	1	1	+	2	2^+
...					

Table 1: Types of mesons

The different types are shown in Table 1. The nonet of the pseudoscalar mesons ($J^P = 0^-$) and the nonet of the vector mesons are shown in Figure 1 and Figure 2. Here the charge increases towards the right and the strangeness increases towards the upward direction. Note, that η and η' are not the exact octet and singlet states, respectively. These are denoted by η_0 and η_8. The physical, measured particles are mixings between the η_0 and η_8 states with an η-η'-mixing angle $\theta_{mix} \approx -20°$ [10]. These states can be constructed from the flavor states according to

$$\begin{pmatrix} \eta \\ \eta' \end{pmatrix} = \begin{pmatrix} -\sin\theta_{\text{mix}} & \cos\theta_{\text{mix}} \\ \cos\theta_{\text{mix}} & \sin\theta_{\text{mix}} \end{pmatrix} \cdot \begin{pmatrix} \eta_0 \\ \eta_8 \end{pmatrix}. \tag{1}$$

Since we want to study the decay of the pseudoscalar mesons π^0, η and η', we first give some general informations of this particles and then show their different decay modes.

The η and η' have a strange quark content:

$$\eta_8 \;:\; \frac{1}{\sqrt{6}}\left(u\bar{u} + d\bar{d} - 2s\bar{s}\right), \tag{2}$$

$$\eta_0 \;:\; \sqrt{\frac{2}{3}}\left(u\bar{u} + d\bar{d} + s\bar{s}\right). \tag{3}$$

The masses of the mesons are $m_\eta = 547.853 \pm 0.024\,\text{MeV}$ and $m_{\eta'} = (957.78 \pm 0.06)\,\text{MeV}$. The decay modes and branching ratios are given in Table 2 and Table 3.

Mode	Branching ratio
$\eta \to 2\gamma$	$(39.30 \pm 0.20) \cdot 10^{-2}$
$\eta \to 3\pi^0$	$(32.56 \pm 0.23) \cdot 10^{-2}$
$\eta \to \pi^0 2\gamma$	$(2.7 \pm 0.5) \cdot 10^{-4}$
$\eta \to \pi^0\pi^0\gamma\gamma$	$< 1.2 \cdot 10^{-3}$
$\eta \to 4\gamma$	$< 2.8 \cdot 10^{-4}$
$\eta \to$ invisible	$< 6 \cdot 10^{-4}$
$\eta \to \pi^+\pi^-\pi^0$	$(22.73 \pm 0.28) \cdot 10^{-2}$
$\eta \to \pi^+\pi^-\gamma$	$(4.60 \pm 0.16) \cdot 10^{-2}$
$\eta \to e^+e^-\gamma$	$(7.0 \pm 0.7) \cdot 10^{-3}$
$\eta \to \mu^+\mu^-\gamma$	$(3.1 \pm 0.4) \cdot 10^{-4}$
$\eta \to e^+e^-$	$< 2.7 \cdot 10^{-5}$
$\eta \to \mu^+\mu^-$	$(5.8 \pm 0.8) \cdot 10^{-6}$
$\eta \to e^+e^-e^+e^-$	$< 6.9 \cdot 10^{-5}$
$\eta \to \pi^+\pi^-e^+e^-$	$(4.2 - 1.3 + 1.5) \cdot 10^{-4}$
$\eta \to e^+e^-\mu^+\mu^-$	$< 1.6 \cdot 10^{-4}$
$\eta \to \mu^+\mu^-\mu^+\mu^-$	$< 3.6 \cdot 10^{-4}$
$\eta \to \mu^+\mu^-\pi^+\pi^-$	$< 3.6 \cdot 10^{-4}$
$\eta \to \pi^+\pi^- 2\gamma$	$< 2.0 \cdot 10^{-3}$
$\eta \to \pi^+\pi^-\pi^0\gamma$	$< 5 \cdot 10^{-4}$
$\eta \to \pi^0\mu^+\mu^-\gamma$	$< 3 \cdot 10^{-6}$

Table 2: branching ratios of the η decays [11]

Mode	Branching ratio
$\eta' \to \pi^+\pi^-\eta$	$(44.6 \pm 1.4) \cdot 10^{-2}$
$\eta' \to \rho_0\gamma$ (including non-resonant $\pi^+\pi^-\gamma$)	$(29.4 \pm 0.9) \cdot 10^{-2}$
$\eta' \to \pi^0\pi^0\eta$	$(20.7 \pm 1.2) \cdot 10^{-2}$
$\eta' \to \omega\gamma$	$(3.02 \pm 0.31) \cdot 10^{-2}$
$\eta' \to \gamma\gamma$	$(2.10 \pm 0.12) \cdot 10^{-2}$
$\eta' \to 3\pi^0$	$(1.61 \pm 0.23) \cdot 10^{-3}$
$\eta' \to \mu^+\mu^-\gamma$	$(1.03 \pm 0.26) \cdot 10^{-4}$
$\eta' \to \pi^+\pi^-\mu^+\mu^-$	$< 2.3 \cdot 10^{-4}$
$\eta' \to \pi^+\pi^-\pi^0$	$(3.7 - 1.0 + 1.1) \cdot 10^{-3}$
$\eta' \to \pi^0\rho^0$	$< 4 \cdot 10^{-2}$
$\eta' \to 2(\pi^+\pi^-)$	$< 2.5 \cdot 10^{-4}$
$\eta' \to \pi^+\pi^-2\pi^0$	$< 2.6 \cdot 10^{-3}$
$\eta' \to 2(\pi^+\pi^-)$ neutrals	$< 1 \cdot 10^{-2}$
$\eta' \to 2(\pi^+\pi^-)\pi^0$	$< 1.9 \cdot 10^{-3}$
$\eta' \to 2(\pi^+\pi^-)2\pi^0$	$< 1 \cdot 10^{-2}$
$\eta' \to 3(\pi^+\pi^-)$	$< 5 \cdot 10^{-4}$
$\eta' \to \pi^+\pi^-e^+e^-$	$(2.5 - 1.0 + 1.3) \cdot 10^{-3}$
$\eta' \to e^+e^-\gamma$	$< 9 \cdot 10^{-4}$
$\eta' \to \pi^0\gamma\gamma$	$< 8 \cdot 10^{-4}$
$\eta' \to 4\pi^0$	$< 5 \cdot 10^{-4}$
$\eta' \to e^+e^-$	$< 2.1 \cdot 10^{-7}$
$\eta' \to invisible$	$< 9 \cdot 10^{-4}$

Table 3: branching ratios of the η' decays [11]

2.2 Symmetries and anomalies

Transformations which do not change the physics of a system are symmetry transformations. In classical physics this means that the action and thereby the equation of motion are unchanged. In a quantum mechanical formulation, a symmetry is given if the Lagrangian is invariant under the respective transformation. The relationship between symmetries and conversation laws is expressed via the Noether theorem which says that for every continuous transformation that leaves the action invariant there exists a time independent classical charge Q and a corresponding conserved current $\partial_\mu J^\mu = 0$.
There exist many different kinds of symmetries, which are all realized by nature. Listed here are two examples:

- exact symmetry: examples for exact symmetries are the electromagnetic gauge $U(1)$ or the $SU(3)$ color symmetry of QCD;

- anomalous symmetry: If a classical symmetry is broken in quantum physics it is called anomalous. It is not a true symmetry. An example is the axial $U(1)$ symmetry, which is the symmetry of interest here.

The concept of anomalies was introduced by Adler, Bell and Jackiw [12, 13]. One will give a short overview of the calculations given in Chapter 19 of [14].
In the massless Dirac Lagrangian the left- and right- handed fermions are decoupled and the Lagrangian is therefore invariant under the transformation of the fields[a]:

$$\Psi \to \Psi' = e^{-i\theta\gamma_5}\Psi \tag{4}$$

The corresponding axial current

$$j_{5\mu} = \bar{\Psi}\gamma_\mu\gamma_5\Psi \tag{5}$$

is classically conserved,

$$\partial^\mu j_{5\mu} = 0. \tag{6}$$

If Ψ satisfies $(i\gamma_\mu\partial^\mu - m)\Psi = 0$, then

$$\begin{aligned}\partial^\mu j_{5\mu} &= (\partial^\mu\bar{\Psi})\gamma_\mu\gamma_5\Psi - \bar{\Psi}\gamma_5\gamma_\mu\partial^\mu\Psi \\ &= (im\bar{\Psi})\gamma_5\Psi - \bar{\Psi}\gamma_5(-im\Psi) \\ &= 2im\bar{\Psi}\gamma_5\Psi = 0\end{aligned}$$

when $m = 0$.

This does not hold quantum mechanically when gauge fields are present. The axial vector current is built from two fermion fields. Because the product of two local operators can induce singularities, we separate their locations x and y, and take the limit $(y - x) \to 0$ in the end. This is visualized in Figure 3.
The lowest order contribution (without background gauge fields) results in zero, because we have to take the trace over three γ-matrices. The next order contribution instead gives a nonvanishing result. Therefore the divergence of the current has the following form,

$$\partial^\mu j_{5\mu} = -\frac{e^2}{16\pi^2}\varepsilon^{\mu\nu\alpha\beta}F_{\mu\nu}F_{\alpha\beta}, \tag{7}$$

which is known as Adler-Bell-Jackiw anomaly [12, 13]. $F_{\mu\nu}$ is the electromagnetic field strength tensor, $F_{\mu\nu} = \partial_\mu A_\nu - \partial_\nu A_\mu$.

The electromagnetic processes influenced by the Abelian axial anomaly [15] are of considerable theoretical interest. Among them are the transitions of the type $\gamma^*(q) \to P^+(p_1)P^0(p_2)P^-(p_3)$, where γ^* denotes a, generally, virtual ($q^2 \neq 0$) photon γ, $P^\pm$ stands for a charged and P^0 for a neutral meson from the pseudoscalar nonet, up to the strangeness conservation (so that $P^\pm = \pi^\pm, K^\pm$ and $P^0 = \pi^0, \eta, \eta'$). These processes are supposedly influenced by the, colloquially called, "box" axial anomaly,

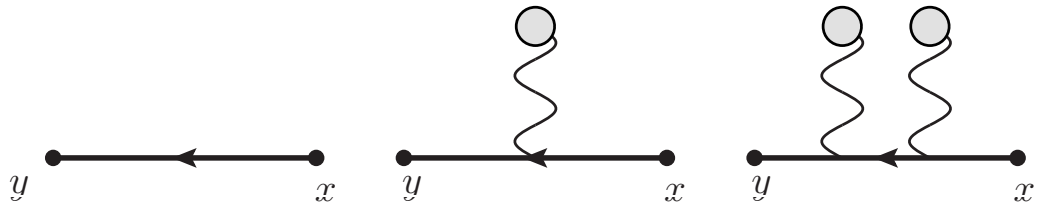

Figure 3: higher order radiative corrections of $\Psi(y)\bar{\Psi}(x)$

since on the microscopic level, the three pseudoscalar (P) mesons would couple to the photon through a four-vertex quark loop, like in Fig. 4.

In the chiral limit (where $m_\pi = 0$) and the soft–point limit (of vanishing 4-momenta of external particles, $p_j = 0 = q$), which is a reasonably realistic approximation at low energies at least for the lightest pseudoscalars – the pions, the anomaly analysis predicts [12] that the theoretical amplitude is exactly

$$A_\gamma^{3\pi} \equiv \lim_{m_\pi \to 0} F_\gamma^{3\pi}(p_1 = 0, p_2 = 0, p_3 = 0) = \frac{e\, N_c}{12\pi^2\, f_\pi^3}\,, \tag{8}$$

where e is the proton charge, N_c the number of quark colors, and the pion decay constant $f_\pi = (92.42 \pm 0.33)$ MeV, whereby $A_\gamma^{3\pi} = (9.72 \pm 0.09)\,\mathrm{GeV}^{-3}$.

[a]The (standard) notation of the γ-matrices is according to [16]. The parameter θ is real valued and $\varepsilon^{\mu\nu\alpha\beta}$ is the total antisymmetric tensor in 3+1 dimensions

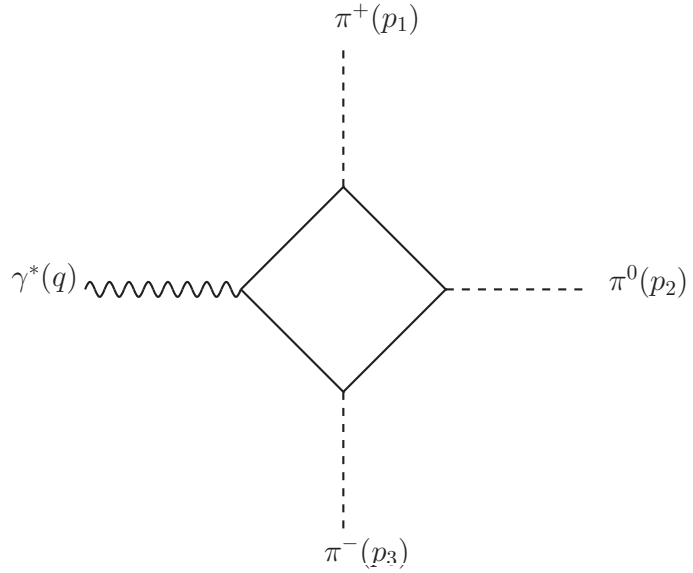

Figure 4: A box diagrams for the process $\gamma^* \to \pi^+\pi^0\pi^-$.

On the other hand, the experimental knowledge of the processes that should be influenced by the "box anomaly" is not at all satisfactory, being quite scant. For the $\gamma^* \to \pi^+\pi^0\pi^-$ processes, which should be best approximated by the anomaly prediction (8) since it involves only the lightest pseudoscalars, there is only one published experimental value for the amplitude at finite momenta p_j, i.e., the form factor $F_\gamma^{3\pi}(p_1, p_2, p_3)$. It was extracted from the cross-section measured [17] at Serpukhov in the transition $\pi^-\gamma^* \to \pi^0\pi^-$ through the Primakoff effect, so that its value $F_\gamma^{3\pi}(expt) = 12.9 \pm 0.9 \pm 0.5\,\mathrm{GeV}^{-3}$ really corresponds to the average value of the form factor over the momentum range covered by the experiment. The π^- scattering on electrons at CERN SPS yielded the total cross section [15] consistent with the Serpukhov value. In the meantime, one still awaits the analysis of the measurements of this form factor performed at CEBAF [18].

Now, however, there are new hopes of more and better experimental knowledge of such processes, as new high-statistic data on the form factor for the $\pi^-\gamma^* \to \pi^-\pi^0$ transition are expected soon from the COMPASS Primakoff experiments at CERN [7].

Thus experiments (including radiative decays of η and η' from g11 and g12) may finally confirm the relation (9) between the "box anomaly" processes and the much better understood and measured "triangle anomaly" processes, notably the $\pi^0(p) \to \gamma(k_1)\gamma(k_2)$ decay into two real photons, $k_1^2 = 0 = k_2^2$. Namely, the pertinent chiral-limit and soft-point amplitudes $A_\pi^{2\gamma}$ and $A_\gamma^{3\pi}$ are related [12] as

$$A_\pi^{2\gamma} \;=\; e f_\pi^2\, A_\gamma^{3\pi}. \tag{9}$$

Wess-Zumino-Witten Lagrangian The Wess-Zumino-Witten Lagrangian consists of terms like:

$$A = \frac{N_c e^2}{96\pi^2 f_\pi^2}\pi^0 \varepsilon^{\mu\nu\alpha\beta} F_{\mu\nu} F_{\alpha\beta}, \tag{10}$$

which is the part that describes the the triangle anormally in the decay $\pi^0 \to \gamma\gamma$, and a term

$$B = -\frac{1}{12}\frac{N_c}{\pi^2 f_\pi^3}\epsilon^{\mu\nu\alpha\beta} A_\mu \partial_\nu \pi^+ \partial_\alpha \pi^- \partial_\beta \pi^0, \tag{11}$$

that describes the coupling of a photon to three pseudoscalar mesons ($\gamma\pi^+\pi\pi^-$ - vertex) and therefore the decays $\eta/\eta' \to \pi^+\pi^-\gamma$.
In summary the Wess-Zumino-Witten Lagrangian already determines the triangle anomaly sector via A and the box anomaly sector via B.

2.3 Radiative Decay Rate

Radiative decays are known to be very sensitive tools to explore decay mechanisms. Especially, when studied together with two hadrons as decay products, they enable us to adjust the invariant mass of the two-hadron system via a variation of the photon energy without interference of strong three-body final state interactions.

For the transitions at hand, the spectral decay data are fitted with a function of the form

$$\frac{d\Gamma(\eta \to \pi^+\pi^-\gamma)}{ds_{\pi\pi}} = |AP(s_{\pi\pi})F_V(s_{\pi\pi})|^2\Gamma_0(s_{\pi\pi}), \tag{12}$$

where the normalization parameter A has the dimension of mass^{-3}, $s_{\pi\pi}$ is the invariant mass squared of $\pi^+\pi^-$ and where

$$\Gamma_0(s_{\pi\pi}) = \frac{1}{3 \cdot 2^{11} \cdot \pi^3 M_\eta^3}(M_\eta^2 - s_{\pi\pi})^3 s_{\pi\pi} \cdot \beta_\pi^3 \tag{13}$$

is the simplest gauge-invariant matrix element multiplied by the phase-space term $\beta_\pi = \sqrt{1 - 4M_\pi^2/s_{\pi\pi}}$ and $F_V(s_{\pi\pi})$ is the pion vector from factor, approximation in the energy range of interest by the polynomial $|F_V(s_{\pi\pi})| = 1 + (2.12 \pm 0.01)s_{\pi\pi} + (2.13 \pm 0.01)s_{\pi\pi}^2 + (13.80 \pm 0.14)s_{\pi\pi}^3$. The $P(s_{\pi\pi})$ function, a process-specific part, can be treated perturbatively in the frame of ChPT, for decay of light mesons. Taylor expansion around $s_{\pi\pi} = 0$ gives

$$P(s_{\pi\pi}) = 1 + \alpha \cdot s_{\pi\pi} + \beta \cdot s_{\pi\pi}^2 + O(s_{\pi\pi}) \tag{14}$$

The parameters α and β allow insights into the physics underlying the decay process.

3 Experimental Setup

The data to be used in this analysis are from part of the g11a experiment, which was taken from May 17 to July 29, 2004, using the CEBAF Large Acceptance Spectrometer (CLAS) located in Hall-B at the Thomas Jefferson National Accelerator Facility (TJNAF). Real photons were produced by bremsstrahlung from a 4.0186 GeV electron beam incident on a 1×10^{-4} radiation length gold foil. The electron beam was delivered by the Continuous Electron Beam Accelerator Facility (CEBAF). The Hall-B Tagging System was used to determine the photon energies by measuring the energies of the recoil electrons using a dipole magnetic field and a scintillator hodoscope. The associated photon energies were then calculated by the difference between the incident electron energies and the recoil electron energies.

A liquid hydrogen target was used in the g11a experiment. The target was contained in a cylindrical Kapton chamber of 2 cm radius and 40 cm length.

The CLAS apparatus was used to detect particles generated from the interaction of the incident photons with the target. The CLAS detector was able to track charged particles that have momenta larger than ∼200 MeV, and the detection area covered polar angles from 8° to 142° and 80% of the azimuthal region. It was composed of several sub-systems, arranged with a six-fold azimuthal symmetry. A plastic scintillator Start Counter, placed just outside of the target, was used to measure the vertex time of particles in coincidence with the incoming photon. The superconducting coils of the CLAS detector generated a toroidal magnetic field that bent

the path of outgoing charged particles. Those particles traveled through 3 regions of drift chambers that measured the curved paths to give the particle momenta. For the g11a experiment, the current in the superconducting coils was set at 1920 A, which gave a maximum magnetic field of $\sim$ 1.8 T. The time of flight (TOF) system was located beyond the outermost drift chambers at a radius of $\sim$4 m from the target and was used to measure the time and position of each charged particle that hit the TOF scintillators. The TOF information, along with the particle momentum, was used for the particle identification in the analysis. The time resolution of the TOF system was about 80 ps to 160 ps, depending on the length of the scintillators.

The event trigger for the g11a experiment required that at least two tracks were detected in different sectors of CLAS. Once the event satisfied this condition, it was written to tape for future analysis.

4 Data Analysis

As one of the largest photoproduction datasets at CLAS, the g11a experiment has $\sim$20 billion triggers.

4.1 Channels of Interest

Because the η and $\eta^{'}$ are unstable, they will quickly decay into the lighter π-mesons and/or γ(s) by the strong interaction. One is interested in the photoproduction channel(s):

$$\gamma p \rightarrow p\eta(\eta^{'}) \tag{15}$$

followed by

$$\eta \rightarrow \pi^{+}\pi^{-}\gamma \tag{16}$$

or

$$\eta^{'} \rightarrow \pi^{+}\pi^{-}\gamma. \tag{17}$$

The η and $\eta^{'}$ are reconstructed using the missing mass technique.

4.2 Event Selection and Particle Identification

Events were selected with three charged tracks in the final state identified as a proton, π^{+} and π^{-} in addition to a photon tagged by an electron in the tagger. These particles were selected according to particle id assigned by the CLAS Simple Event Builder (SEB) package. In order to identify the type of particle, the SEB package calculates the velocity β_{meas} of the detected particle and compares it with the expected β_{cal} corresponding to the measured momentum and the masses of different possible types of particles. The particle type is chosen based on the minimum difference between the measured β_{meas} and β_{cal} velocities.

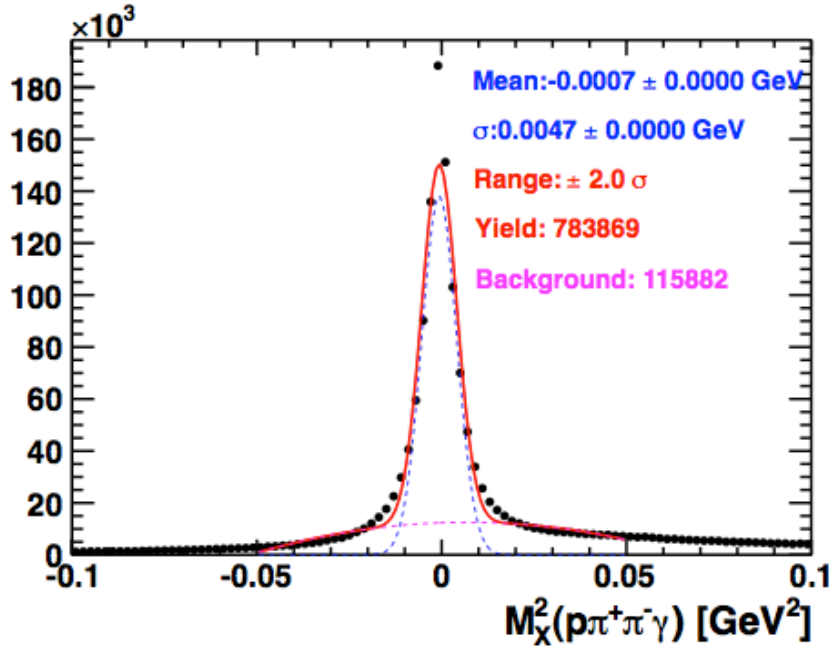

Figure 5: Missing mass $M_X(p\pi^+\pi^-\gamma)$ of all detected final state particles.

4.3 Cuts

The decay of a pseudoscalar meson to $\pi^+\pi^-\gamma$ requires identification of final state separation of single photon from π^0.

Several cuts were applied to the data to reduce the background and to remove events below threshold for the reaction of interest. In general, the strategy is to use kinematic constraints to eliminate backgrounds while ensuring that the signal remains robust. The efficiency of various cuts would later on be tested with Monte Carlo simulations.

The kinematic constraints used so far are listed below:

- Figure 5 shows the missing mass of all detected particles with a cut on missing energy $|ME - E_\gamma| < 0.05$ GeV. This plot shows a peak around zero, but it doesn?t yet secure rejection of π^0 in the event.

- To ensure there is a π^0 amongst p, π^+ and π^- in the final state, the square of the missing mass $M(p\pi^+\pi^-)^2$ with additional cut $M(p\pi^+\pi^-\gamma)^2 < 0.01$ GeV^2 for different ranges of missing mass $M_X(p)$ in the range of η, ρ/ω and $\eta^{'}$ is plotted (Figure 6). One can clearly see the peaks of single γ and π^0.

- Reconstruction of all particles of interest with the best resolution was obtained by plotting the missing mass $M_X(p)$ with the cuts $M_X^2(p\pi^+\pi^-\gamma) < 0.01$ GeV^2 and $M_X^2(p\pi^+\pi^-) < 0.005$ GeV^2, Figure 7.

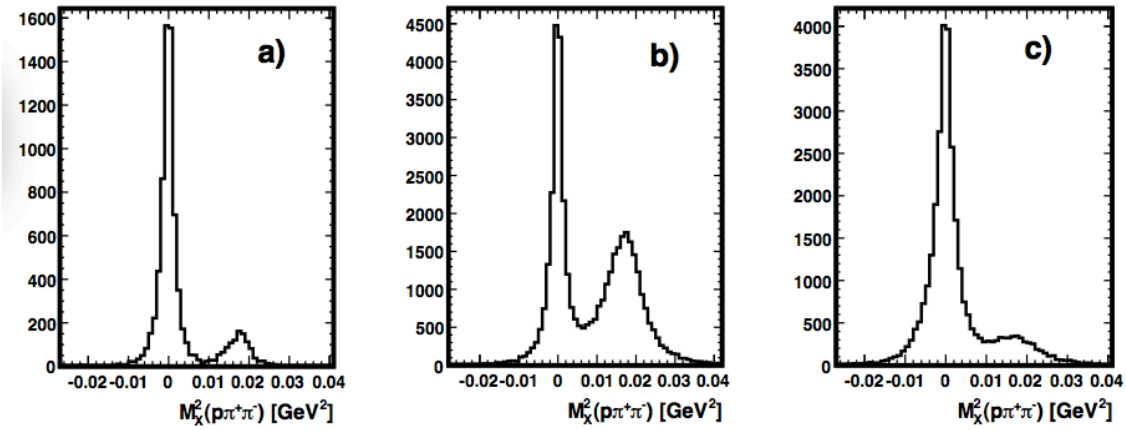

Figure 6: Distribution of events vs missing mass squared $M_X^2(p\pi^+\pi^-\gamma)$ for the range: a) $M_X(p) = 0.55 \pm 0.02$ GeV; b) $M_X(p) = 0.76 \pm 0.06$ GeV; c) $M_X(p) = 0.96 \pm 0.02$ GeV.

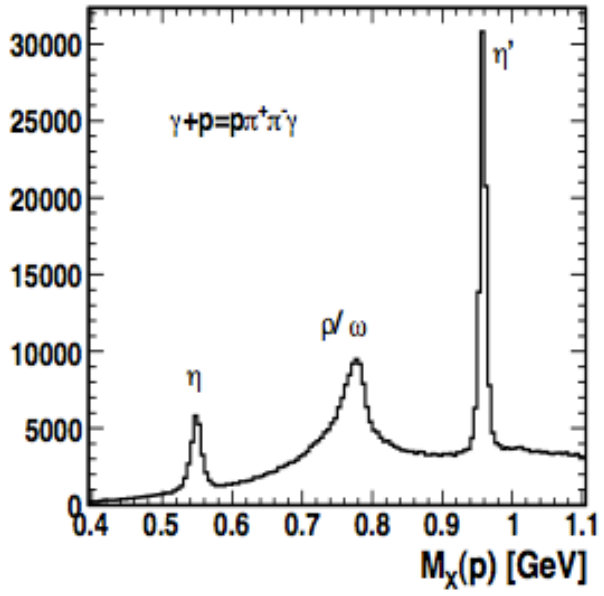

Figure 7: Distribution of missing mass of the proton in the exclusive reaction $\gamma p \to p\pi^+\pi^-\gamma$.

5 CLAS preliminary versus world data

Figure 7 represents the missing mass of the proton from g11 dataset for the exclusive reaction $\gamma p \to p\pi^+\pi^-\gamma$. In both the η and $\eta^{'}$ peaks, the statistics is more than an order of magnitude higher than existing world data [19].

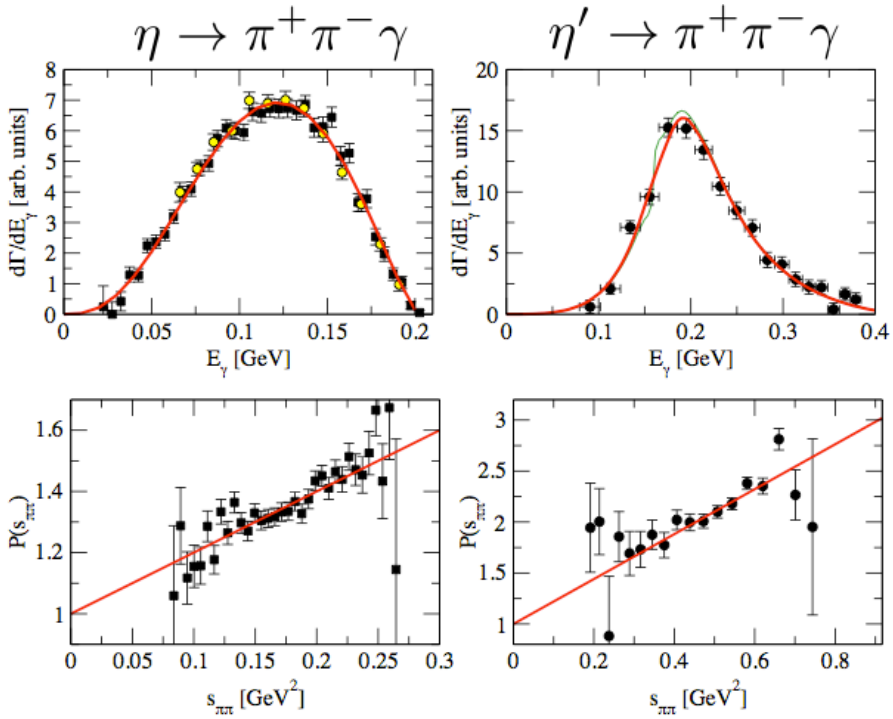

Figure 8: Top-left panel: distribution of E_γ in cm frame of η. Top-right panel: same for $\eta^{'}$. Experimental data are from [20, 21]. Lower panel: Plot of $P(S_{\pi\pi})$, as extracted from the experimental data above.

Figure 8 shows the center-of-mass photon energy distribution, E_γ^{cm} for η (top-left panel) and $\eta^{'}$ (top-right panel) from [20, 21]. The Lower panel shows plots of $P(S_{\pi\pi})$, Eqs.(12) and (14), as extracted from the experimental the mentioned experimental data.

The fits to the data points of the WASA-at-COSY collaboration [20] for η case and the CRYSTAL BARREL collaboration [21] for the η' case give values:
$\alpha = (1.96 \pm 0.27 \pm 0.02)$ GeV^{-2} and $\alpha' = (1.80 \pm 0.49 \pm 0.04)$ GeV^{-2} respectively.

Figure 9 shows the center-of-mass photon energy distribution, E_γ^{cm} for η (top-left panel) and η' (top-right panel). The lower panels shows $s_{\pi\pi}$ for η and η' from the CLAS g11 dataset before acceptance and efficiency corrections. $s_{\pi\pi}$ and E_γ^{cm} are related by the expression:

$$s_{\pi\pi} = m^2 - 2E_\gamma m \tag{18}$$

where $m = m_\eta(m_{\eta'})$.

Figure 10 shows the value of α extracted from five data points for the radiative decay of η. One is currently working on increasing the data points and extending the $s_{\pi\pi}$ range to around 0.25 GeV^2. With a projection to reduce the statistical error

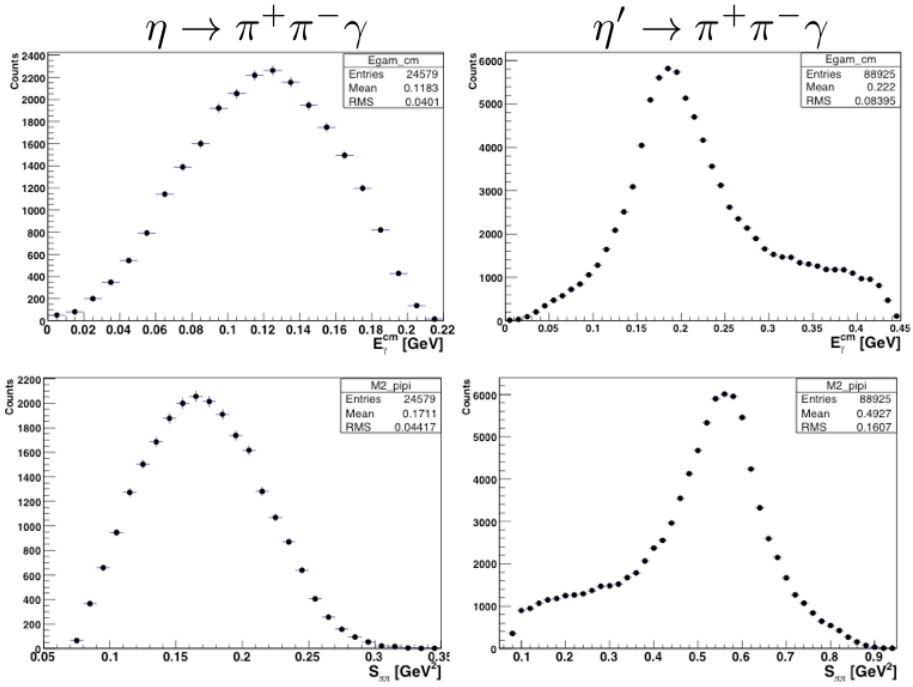

Figure 9: Top-left panel: distribution of E_γ in cm frame of η. Top-right panel: same for $\eta^{'}$. Lower-left panel: distribution of E_γ in cm frame of η. Lower-right panel: same for $\eta^{'}$. Experimental data are from CLAS g11 data before acceptance and efficiency corrections.

to about that of the most recent result, $\alpha = (1.32 \pm 0.08 \pm 0.02)$ GeV^{-2}, from the KLOE Collaboration [23]. A similar procedure would be carried out for the η' decay, in CLAS. This measurement would provide the best statistical precision for α' till date.

6 Expectations and Conclusion

In conclusion, from the preliminary analyses done so far one can see that the CLAS data on the radiative decay of pseudoscalar mesons has high statistics compared to world data and can contribute significantly to essential topics of low energy QCD.

Ones immediate expectation is to use Monte Carlo simulations to carry on with acceptance and efficiency corrections so as to calculate the differential cross sections of the processes $\eta \to \pi^+\pi^-\gamma$ and $\eta' \to \pi^+\pi^-\gamma$. Followed by making measurements of E_γ^{cm} and $s_{\pi\pi}$ distributions in both processes and hence extract the model-independent α and α' parameters.

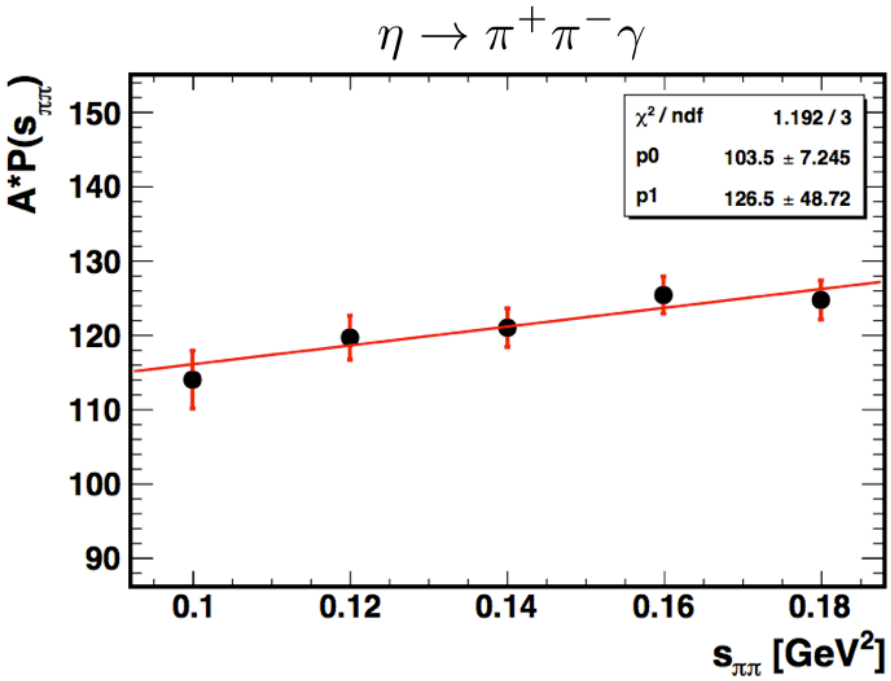

Figure 10: Very preliminary value for $\alpha = (1.22 \pm 0.47)$ GeV^{-2} before acceptance and efficiency corrections.

References

[1] N. P. Samios, Phys. Rev. **121**, 275 (1961).

[2] A. Bedall, Eur. Phys. J. **C54**, 365 (2008).

[3] A. R. Barker *et al.*, Phys. Rev. **D67**, 033008 (2003).

[4] C. C. Lih, ARXIV:0912.2147

[5] M. Berlowski *et al.*, Phys. Rev. **D77**, 032004 (2008).

[6] KLOE, F. Ambrosino *et al.*, (2008), ARXIV:0812.4830

[7] P. Abbon *et al.* [COMPASS Collaboration], Nucl. Instrum. Meth. A **577**, 455 (2007) [arXiv:hep-ex/0703049].

[8] J. Wess and B. Zumino, Phys. Lett. **B37**, 95 (1971).

[9] E. Witten, Nucl. Phys. **B223**, 422 (1983).

[10] B. R. Holstein, Phys. Scripta **T99**, 55 (2002), hep-ph/0112150

[11] Particle Data Group, C. Amsler *et al.*, Phys. Lett. B667, 1 (2008).

[12] S. L. Adler, Phys. Rev. **177**, 2426 (1969).

[13] J. S. Bell *et al.*, **A60**, 47 (1969).

[14] M. E. Peskin, D. V. Schroeder, *An Introduction to Quantum Field Theory* (Addison-Wesley, USA, 1995).

[15] S. Benić it et al., arXiv: 1109.3140

[16] J. D. Bjorken and S. D. Drell, Bibliograph Inst./Mannheim 1967.

[17] Y. M. Antipov, V. A. Batarin, V. A. Bezzubov, N. P. Budanov, Y. P. Gorin, Y. A. Gornushkin, S. P. Denisov, S. V. Klimenko *et al.*, Phys. Rev. **D36** (1987) 21.

[18] R. A. Miskimen, K. Wang, A. Yagneswaran (spokesmen),"Study of the Axial Anomaly using the $\gamma\pi^+ \to \gamma\pi^+$ Reaction Near Threshold", letter of intent, CEBAF-experiment 94-015.

[19] M. J. Amaryan *et al.*, Photoproduction and Decay of Light Mesons in CLAS.

[20] P. Adlarson *et al.* (WASA@COSY Collaboration), Phys. Lett. **B707**, 243 (2012), 1107.5277.

[21] A. Abele *et al.* (Crystal Barrel Collaboration), Phys. Lett. **B402**, 195 (1997).

[22] F. Stollenwerk *et al.* arXiv: 1108.2419v3 (2011).

[23] D. Babusci *et al.* arXiv: 1209.4611v2 (2012).